Experimental and theoretical studies for steel XC38 corrosion inhibition in 1 M HCl by *N*-(8-hydroxyquinolin-5-yl)-methyl)-*N*-phenylacetamide

M. El Faydy[1], M. Galai[2], R. Touir[2,3,]*, A. El Assyry[4], M. Ebn Touhami[2], B. Benali[4], B. Lakhrissi[1], A. Zarrouk[5]

[1]*Laboratoire d'Agroressources, Polymères et Génie des Procédés, Département de Chimie, Université Ibn Tofail, B.P. 133 Kénitra, Morocco*

[2]*Laboratoire d'ingénierie des Matériaux et d'Environnement : Application et Modélisation, Département de Chimie, Université Ibn Tofail, B.P. 133 Kénitra, Morocco.*

[3] *Centre Régional des métiers de l'éducation et de la formation (CRMEF), Avenue Allal Al Fassi, Madinat Al Irfane, BP 6210 Rabat, Morocco.*

[4]*Laboratoire d'Optoélectronique et de Physico-chimie des Matériaux (Unité associée au CNRST), Département de Physique, Université Ibn Tofail, B.P. 133 Kénitra, Morocco*

[5] *LC2AME, Faculty of Science, First Mohammed University, PO Box 717, 60 000 Oujda, Morocco*

Abstract

In the present investigation, a new organic inhibitor, namely *N*-((8-hydroxyquinolin-5-yl) methyl)-*N*-phenylacetamide (HQMP) was synthesized and characterized using ^{1}H, ^{13}C NMR and IR spectroscopies. In the second time, the inhibition effect of HQMP on the steel XC38 corrosion in 1 M HCl, have been investigated using electrochemical measurements. The obtained results showed that the its inhibition efficiency increased with concentration and reached 93 % at 10^{-3} M. in addition, the HQMP takes its performance at the temperature range of 298–328 K. The adsorption of the inhibitor on the mild steel was well described by the Langmuir isotherm. On the other hand, the establishing of correlation between the molecular structure of quantum chemistry indices was carried out using the density functional theory (DFT).

*Keywords:*8-Quinolinol, *N*-phenylacetamide, Synthesis, Steel XC38, Corrosion inhibition, Acidic medium, DFT

1. Introduction

From an economic point of view the corrosion is of a great importance. We consider for example that every year the quarter of the production of steel is destroyed by the corrosion; these losses could be superior if there was no protection against the corrosion. Steel is one of the most widely used metals in our modern world, building materials, roads, and bridges [1-3]. Its versatility, durability, and strength make it a popular choice for many different applications, Acid solution are often used in industry for cleaning, descaling and pickling of metallic structures, processes which are normally accompanied by considerable dissolution of the metal, for that reason we need to protect the steel against the corrosion we use inhibitors of corrosion. The action of such inhibitors depends on the molecular structure of the inhibitor Organic compounds, containing functional electronegative groups and π-electron in triple or Conjugated double bonds are usually good inhibitors. Heteroatom's, such as (S, N, Se, O, P), together with aromatic rings in their structure are the major adsorption centers [4-9]. Recently, various compounds based of 8-hydroxyquinoline have been used as good inhibitors for mild steel. Therefore, quinoline (nitrogen – heterocyclic) can be regarded as excellent corrosion inhibitors [10, 11].

The aim of the present work was to synthesize, characterize and study the performance of *N*-((8-hydroxyquinolin-5-yl)-methyl)-*N*-phenylacetamide on the corrosion inhibition of steel XC38 in 1 M HCl. Correlation between the quantum chemical calculations and molecular structure was discussed using density functional theory (DFT).

2. **Experimental**

2.1. Materials

Steel XC38 containing in wt. %: 0, 37 C, 0.23 Si, 0.68 Mn, 0,016 S, 0,077 Cr, 0,011 Ti, 0,059 Ni, 0,009 Co, 0.16 Cu, and balance iron was used for weight-loss and electrochemical tests. For weight loss measurements, the rectangular coupons with the size of 5 cm × 1 cm × 0.1 cm were used. A columned C38 steel specimen, embedded in Teflon holder using epoxy resin with an exposed area of 1 cm^2, was used as the working electrode for electrochemical measurements. The coupons and electrodes were abraded with emery paper (up to 1200 grit), cleaned with acetone and washed with distillated water, and finally dried at hot air before being immersed in the acid solution. The aggressive solution was prepared by dilution of an analytical grade HCl solution (37 %) with distilled water. The concentration of inhibitors was ranged from 10^{-6} to 10^{-3} M. All assessments were carried out at temperature 298 ± 1 K.

For the synthesis of *N*-((8-hydroxyquinolin-5-yl)-methyl)-*N*-phenylacetamide (HQMP), all chemicals were purchased from Aldrich or Acros (France). The melting points were determined on an automatic electrothermal IA 9200 digital. ^{1}H and ^{13}C NMR spectra were recorded on a Bruker 300 WB spectrometer at 300 MHz, for solutions in Me$_2$SO-d$_6$. Chemical shifts are given as δ values with reference to tetramethylsilane (TMS) as internal standard.

Infrared spectra were recorded from 400 cm^{-1} to 4000 cm^{-1} on a Bruker IFS 66v Fourier transform spectrometer using KBr pellets. So, the 5-chloromethyl-8-quinolinol hydrochloride (I) (Figure 1) was prepared according to method reported in literature [12]. Secondly, *N*-Phenylacetamide (II) (Figure 2) was synthesized according to the method reported in the literature [13].
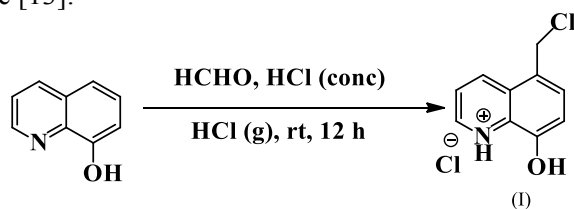

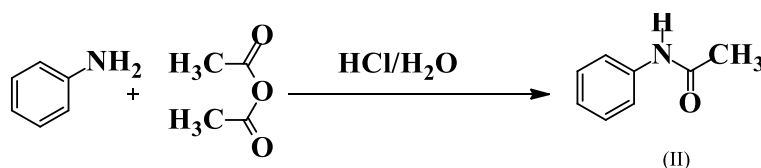**Figure 1:** 5-Chloromethyl-8-quinolinol hydrochloride (I)

Figure 2: *N*-Phenylacetamide (II)

Finally, *N*-((8-hydroxyquinolin-5-yl) methyl)-*N*-phenylacetamide (HQMP) (Figure 3), was synthesized from 5-chloromethyl-8-hydroxyquinoline hydrochloride (I) and *N*-phenylacetamide (II) following the procedure described below:
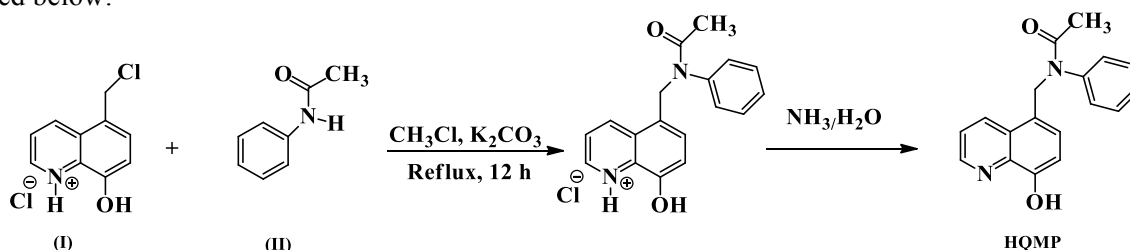

Figure 3: *N*-((8-hydroxyquinolin-5-yl)-methyl)-*N*-phenylacetamide (HQMP)

The mixture of 1 g (4.3 mmol) of 5-chloromethyl-8-quinolinol hydrochloride (**I**), 0.58 g (4.3 mmol) of *N*-phenylacetamide (**II**) and (0.92 g, 8.6 mmol) of K_2CO_3 in chloroform was refluxed for 12 hours. The progress of the reaction was monitored by TLC using hexane-acetone (4:6, v/v) as eluent. The precipitate was filtrated and washed by distilled water and the yellow residue was treated with dilute ammonia. The white solid formed was filtered, dried and recrystallized from benzene-ethyl acetate (2:1, v/v). The structure of the new prepared product (HQMP) was confirmed by ^{1}H NMR and ^{13}C NMR spectra.

2.2. *Electrochemical methods*

A silver chloride electrode (Ag/AgCl) was used as a reference electrode and all potentials were given with it. The counter electrode was a platinum plate of large surface area.

In addition, the working electrode was immersed in the test solution during half an hour until a steady state open circuit potential (E_{ocp}) was obtained. The steady-state polarization curves were recorded potentiodynamically using a VoltaLab PGZ 100 and controlled by a personal computer. The cathodic polarization curve was recorded by polarization from E_{ocp} to negative direction under potentiodynamic conditions corresponding to 1 mV s^{-1} (sweep rate) and under air atmosphere. After this scan, the anodic polarization curve was recorded by polarization from E_{ocp} to positive direction under the same conditions as said before. To evaluate corrosion kinetic parameters, a fitting by Stern-Geary equation was used. To do so, the overall current density values, *i,* were considered as the sum of two contributions, anodic and cathodic current i_a and i_c, respectively. For the potential domain not too far from the open circuit potential, it may be considered that both processes followed the Tafel law [21]. Thus, it can be derived from equation (1):

$$i = i_a + i_c = i_{corr}\left\{\exp\left[b_a \times \left(E - E_{corr}\right)\right] - \exp\left[b_c \times \left(E - E_{corr}\right)\right]\right\} \tag{1}$$

where i_{corr} is the corrosion current density (A cm^{-2}), b_a and b_c are the Tafel constants of anodic and cathodic reactions (V^{-1}), respectively. These constants are linked to the Tafel slopes β (V/dec) in usual logarithmic scale given by equation (2):

$$\beta = \frac{\ln 10}{b} = \frac{2.303}{b} \tag{2}$$

The corrosion parameters were then evaluated by means of nonlinear least square method by applying equation (2) using Origin software. However, for this calculation, the potential range applied was limited to ±0.100V around E_{corr}, else a significant systematic divergence was sometimes observed for both anodic and cathodic branches.

The corrosion inhibition efficiency is evaluated from the corrosion current densities values using the relationship (3):

$$\eta_{PP} = \frac{i^0_{corr} - i_{corr}}{i^0_{corr}} \times 100 \tag{3}$$

Where i^0_{corr} and i_{corr} are the corrosion current densities values without and with inhibitor, respectively.

The electrochemical impedance spectroscopy measurements were carried out using a transfer function analyzer (VoltaLab PGZ 100), with a small amplitude a.c. signal (10 mV rms), over a frequency domain from 100 kHz to 100 mHz with five points per decade. The EIS diagrams were done in the Nyquist representation. The results were then analyzed in terms of an equivalent electrical circuit using Bouckamp program [22].

The inhibiting efficiency derived from EIS, η_{EIS} is also added in Table 4 and calculated using the following equation (4):

$$\eta_{EIS} = \frac{R_{ct} - R^0_{ct}}{R_{ct}} \times 100 \tag{4}$$

where R^0_{ct} and R_{ct} are the charge transfer resistance values in the absence and in the presence of inhibitor, respectively.

2.3. *Quantum chemical calculations*

Density Functional theory (DFT) has been recently used [14, 17] to describe the interaction between the inhibitor molecule and the surface as well as the properties of these inhibitors concerning their reactivity. The molecular band gap was computed as the first vertical electronic excitation energy from the ground state using the time-dependent density functional theory (TD-DFT) approach as implemented in Gaussian 03 [18]. For these seek, some molecular descriptors, such as HOMO and LUMO energy values, frontier orbital energy gap, molecular dipole moment, electronegativity (χ), global hardness (η), softness (S), the fraction of electron transferred (ΔN), were calculated using the DFT method and have been used to understand the properties and activity of the newly prepared compounds and to help in the explanation of the experimental data obtained for the corrosion process.

According to Koopman's theorem [19] the ionization potential (IE) and electron affinity (EA) of the inhibitors are calculated using the following equations (IE = -E_{HOMO}; EA = -E_{LUMO}).

Thus, the values of the electronegativity (χ) and the chemical hardness (η) according to Pearson, operational and approximate definitions can be evaluated using the following relations [20]:

$$\chi = \frac{IE + EA}{2} \qquad (5)$$

$$\eta = \frac{IE - EA}{2} \qquad (6)$$

The number of transferred electrons (ΔN) was also calculated depending on the quantum chemical method [21, 22] by using the equation:

$$\Delta N = \frac{\chi_{Fe} - \chi_{inh}}{2(\eta_{Fe} - \eta_{inh})} \qquad (7)$$

where χ_{Fe} and χ_{inh} denote the absolute electronegativity of iron and inhibitor molecule, η_{Fe} and η_{inh} denote the absolute hardness of iron and the inhibitor molecule respectively. In this study, we use the theoretical value of ($\chi_{Fe} = 7.0\ eV$) and ($\eta_{Fe} = 0$), for calculating the number of electron transferred.

3. **Results and discussion**

3.1. *Characterization of HQMP*

The *N*-((8-hydroxyquinolin-5-yl) methyl)-*N*-phenylacetamide (HQMP) was obtained as a white solid in 85 % yield (0.41 g), mp > 260°C.

The IR, ^{1}H and ^{13}C NMR spectra were used to characterize and confirm the obtained product structure (See Supplementary data) (Table 1).

Table 1. Spectral data of the synthesized compounds

Spectral data
IR (KBr) λ cm^{-1}: 3615 (aromatic-OH bonded), 1634 (-C=O), 1502-1461 (C=C aromatic), 1270 (aromatic C-N), 1065-1156 (-CH$_2$-N)
^{1}H NMR (300 MHz, DMSO-d$_6$) δppm: 7.01-8.54 (multiplet, quinoline and benzene), 8.51-8.54 (doublet, quinoline H-C=N), 6.97-7.01 (doublet, quinoline H-C=C-O), 4.75 (doublet, quinoline -CH$_2$-N), 9.94(singlet quinoline C-OH), 2.03 (singlet of H$_3$C-C).
^{13}C NMR (300 MHz, DMSO-d$_6$) δppm: 24.43 (-CH$_3$), 65.18 (quinoline-CH$_2$-N), 110.99-138.15 (Aromatic: quinoline and benzene), 139.80 (benzene C-N), 147.92 (quinoline C=N), 153.10 (quinoline C-OH), 168.77 (N-C=O)

3.2. *Potentiodynamic polarization curves*

Potentiodynamic polarization curves for steel XC38 in 1 M HCl in the absence and presence of different concentration of HQMP at 298 K are shown in Figure 8. The examination of this Figure allows noting that the addition of HQMP pulls an important decrease of corrosion rate for all the concentrations and the values of

corrosion potential (E_{corr}) and anodic Tafel slope (β_a) change when the concentration increases. In addition it is noted that both anodic and cathodic currents were decreased with HQMP concentration indicating that the HQMP reduces anodic dissolution and also retards the hydrogen evolution reaction.

As well, Table 1 gives the values of kinetic corrosion parameters as the corrosion potential E_{corr}, corrosion current density i_{corr}, anodic and cathodic Tafel slope (β_a and β_c), and inhibition efficiency. It is clear that the addition of HQMP leads to decrease of the current density and the inhibition efficiency increases with inhibitor concentration to reach 93 % at 10^{-4} M. this can be explained by the adsorption of the compounds organic on the metal surface.
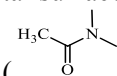
So, the high inhibition efficiency for HQMP, was attributed to the presence of electron donor groups ( ) in their structure. The adsorption of HQMP on the metal surface can occur either directly on the basis of donor–acceptor interactions between the π-electrons of the ring and the vacant d-orbital of steel XC38 surface atoms or an interaction of organic nitrogen compounds with already adsorbed groups as proposed in literature [23, 24].
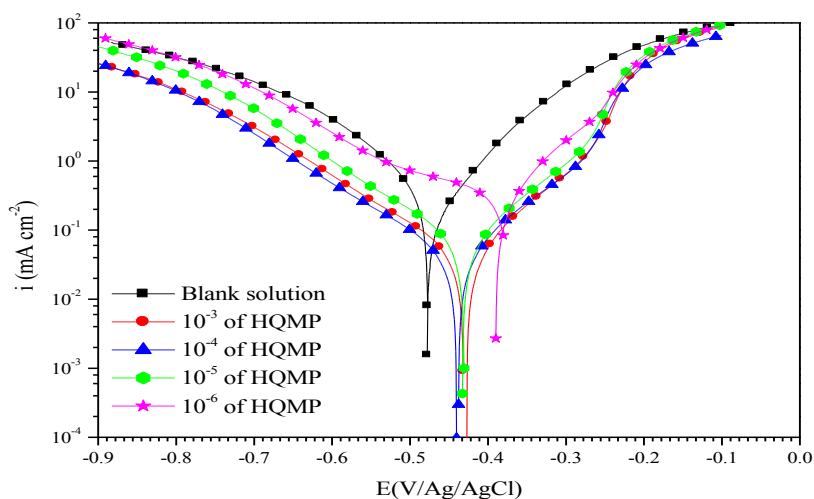

Figure 8: Potentiodynamic polarization curves of steel XC38 in 1M HCl solution containing different concentration of HQMP at 298 K

Table 1: Electrochemical parameters of steel XC38 in 1 M HCl solution in the absence and presence of different concentrations of HQMP

Inhibitor	Conc. (M)	E_{corr} (mV/Ag/AgCl)	i_{corr} ($\mu A\ cm^{-2}$)	β_a (mV dec^{-1})	β_c (mV dec^{-1})	η_{PP} (%)
Blank	00	-498	467	125	-170	-
HQMP	10^{-6}	-367	91	66	-191	88
	10^{-5}	-419	55	85	-153	88
	10^{-4}	-430	33	78	-135	93
	10^{-3}	-420	43	69	-125	91

3.3. *Electrochemical impedance spectroscopic studies*

The corrosion behaviour of steel XC38 in 1 M HCl solution in the absence and presence of different concentrations of HQMP is also investigated by EIS method at E_{corr} and at 298 K after 30 min of immersion. The representative Nyquist plots is shown in Figure 9 and its extracted parameters are presented in Table 2. It is noted that the Nyquist plot of steel XC38 in the absence and presence of inhibitor contains a slightly depressed semi-circular shape and

only one time constant was appeared indicating that the steel XC38 corrosion is mainly controlled by a charge transfer process. In this case, the equivalent electric circuit, Figure 10, with one time constants was proposed to reproduce these results by non linear regression calculation. However, it is seen that the R_{ct} values increased and C_{ct} values decreased with inhibitor concentration. These can be due to the decrease in local dielectric constant and/or increase in thickness of the electrical double layer, suggesting that HQMP acts via adsorption at the metal / solution interface [25, 26].
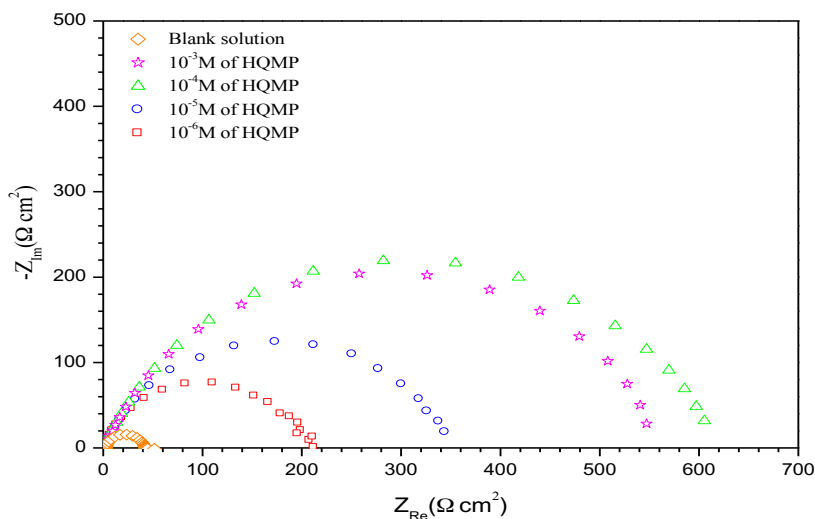

Fig. 9: Nyquist plots for steel XC38 in 1 M HCl solution in the absence and presence of different concentrations of HQMP
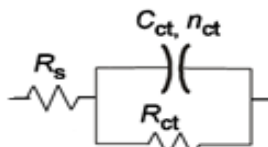

Figure 10: Electrical equivalent circuits used for modeling the metal/solution interface.

Table 2: Electrochemical data of EIS for steel XC38 in 1 M HCl in the absence and presence of different concentrations of HQMP.

Inhibitor	Conc. (M)	R_{ct} (Ω cm^2)	C_{dl} (μF cm^{-2})	η_{EIS} (%)
Blank	00	40.0	295.0	-
	10^{-6}	208.5	99.3	81
	10^{-5}	348.0	94.0	89
HQMP	10^{-4}	615.0	74.0	94
	10^{-3}	559.8	12.1	93

3.4. Effect of temperature

To investigate the mechanism of inhibition and to calculate the activation energies of the corrosion process, Potentiodynamic polarization measurements were taken out at various temperatures range 298–348 K in the absence and presence of inhibitor at 10^{-4} M of HQMP, during 30 minutes of immersion. The obtained results are presented the Figure 11 and 12. The corresponding data are shown in Table 3. It is noted that the i_{corr} increases with temperature in the absence and the presence of HQMP. This can be explained that the dissolution of steel

XC38 is more important than the inhibitor adsorption. In addition, the activation energy for the corrosion process was estimated from Arrhenius type plot according to the following equations and its transition state:

$$i_{corr} = A\exp(\frac{-E_a}{RT}) \qquad (9)$$

Where E_a is the apparent activation energy, A is the Arrhenius factor, N is the Avogadro's number, h is the Plank's constant, R is the universal gas constant and T is the absolute temperature.
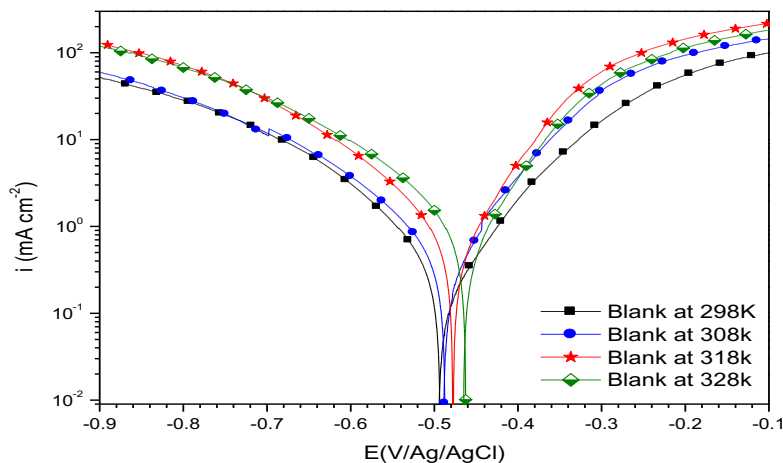

Figure 11: Potentiodynamic polarization curves for steel XC38 in 1 M HCl at different temperatures
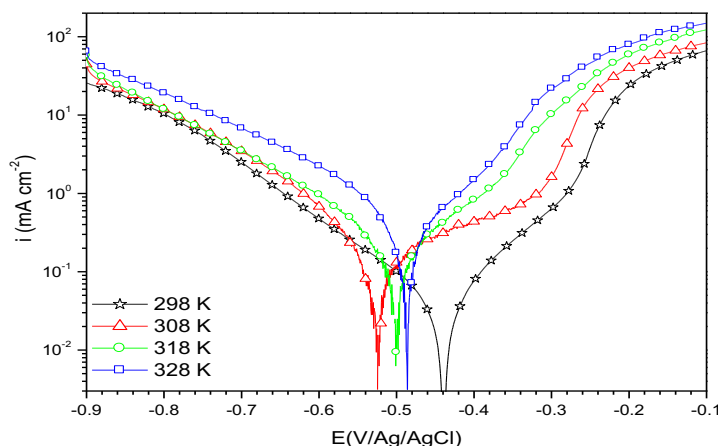

Figure 12: Potentiodynamic polarization curves for steel XC38 in 1 M HCl+10^{-4} M of HQMP at different temperatures

The plots of logarithm of the corrosion current density versus reciprocal temperature T^{-1} are given in Figure 13. The obtained plots are straight lines and the slope of each one gives its activation energy E_a. It is observed that for the corrosion of steel XC38 in 1 M HCl, the E_a value was found equal to 34.61 kJ mol^{-1}. In the presence of 10^{-4} M of HQMP, the E_a value is higher and equal to 50.68 kJ mol^{-1}. The change of the values of the apparent activation energies may be explained by the modification of the mechanism of the corrosion process in the presence of adsorbed inhibitor molecules [27].

Table 3: Electrochemical parameters of steel XC38 in 1 M HCl in the absence and presence of 10^{-4} M of HQMP at different temperatures

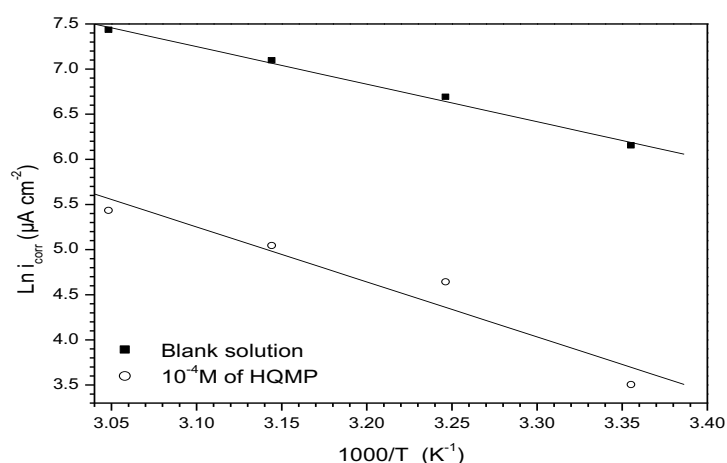|	T (K)	E_{corr} (mV/Ag/AgCl)	i_{corr} (μA cm^{-2})	β_c (mV dec^{-1})	η_{PP} (%)
Blank	298	- 498	467	- 170	-
	308	- 491	800	- 178	-
	318	- 475	1200	- 165	-
	328	- 465	1680	- 151	-
10^{-4} M of HQMP	298	- 437	0.467	- 135	93
	308	- 525	0.8	- 94	87
	318	- 500	1.2	- 98	87
	328	- 488	1.68	- 105	86

Figure 13: Arrhenius plots of steel XC38 in 1 M HCl without and with 10^{-4} M of HQMP.

3.5. *Adsorption isotherm*

Generally, inhibitors may function by physisorption, chemisorptions or by complexation with metal ions. The adsorption isotherm type can provide additional information about the properties of tested compounds. However, the coverage surface (θ) can be easily determined from ac impedance, polarization or weight loss measurements by the ratio *η/100*.

In this study, the coverage surface is estimated from potentiodynamic polarization measurements to make the fitting and select the suitable isotherm. The following adsorption isotherms are the most common models to study the mechanism of corrosion inhibition [28, 29]:

Tempkin adsorption isotherm $\qquad\qquad \exp(f \times \theta) = K_{ads} \times C_{inh} \qquad\qquad$ (9)

Langmuir adsorption isotherm $\qquad\qquad \dfrac{\theta}{1-\theta} = K_{ads} \times C_{inh} \qquad\qquad$ (10)

Frumkin adsorption isotherm $\qquad\qquad \dfrac{\theta}{1-\theta}\exp(-2 \times f \times \theta) = K_{ads} \times C_{inh} \qquad\qquad$ (11)

Freundlich adsorption isotherm $\qquad\qquad \theta = K_{ads} \times C_{inh} \qquad\qquad$ (12)

Flory–Huggins adsorption isotherm $\qquad\qquad \log(\dfrac{\theta}{C_{inh}}) = \log(K_{ads}) + a \times \log(1-\theta) \qquad\qquad$ (13)

where K_{ads} is the equilibrium constant of the adsorption process, C_{inh} is the inhibitor concentration, f is the factor of energetic inhomogeneity and the parameter 'a' in Equation (13) is the number of water molecules replaced by inhibitor molecules on metal surface.

For each inhibitor, a Tempkin, Langmuir, Frumkin, Freundlich and Flory–Huggins isotherm were fitted. It is found that the best fit shows that the inhibitor is adsorbed on metallic surface according to the Langmuir isotherm model. In addition, Figure 14 shows the relationship between C_{inh}/θ and C_{inh} (Langmuir isotherm) for HQMP. From the intercepts of the straight lines C_{inh}/θ vs. C_{inh}, the equilibrium constant values of the adsorption process, K_{ads} can be determined. This constant is related to the free energy of adsorption, ΔG^*_{ads}, by the following equation [30]:

$$K_{ads} = \frac{1}{55.55}\exp(\frac{-\Delta G^*_{ads}}{RT}) \tag{14}$$

where 55,55 value represents the water concentration in solution by mol L^{-1}, R is the universal gas constant and T is the absolute temperature.

The free energy of adsorption, ΔG^*_{ads} can be calculated. It is well known that ΔG^*_{ads} values on the order of - 20 kJ mol^{-1} or less indicate a physisorption, while those more negative than - 40 kJ mol^{-1} involve charge sharing or transfer from the inhibitor molecules to the metal surface to form a coordinate chemical bond (chemisorptions), while values between -20 kJ mol^{-1} and - 40 KJ mol^{-1} indicate both physisorption and chemisorption [31]. In our case, ΔG^*_{ads} values is -47.80 KJ mol^{-1}. This value indicated that adsorption of HQMP occurs via both chemisorption and physisorption [32, 33].
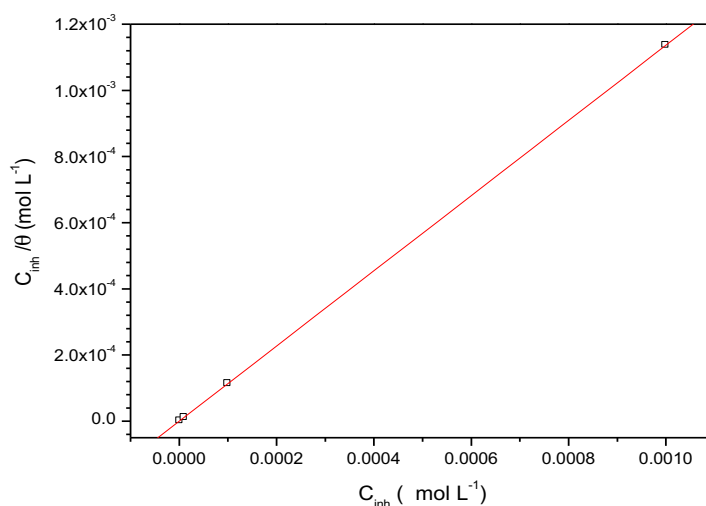

Figure 14: Plot of Langmuir adsorption isotherm of HQMP on the steel XC38 surface at 298 K.

3.6. *Computational procedures*
Computational methods have a strong impact toward the design and development of organic corrosion inhibitors. Recently, density function theory (DFT) has been used to analyze the characteristics of the inhibitor/surface mechanism and to describe the structural nature of the inhibitor on the corrosion process. Furthermore, DFT is considered to be a very useful technique to probe the inhibitor/surface interaction as well as to analyze the experimental data [34]. Thus in our present investigation, DFT method was employed to give some insight into the inhibition action of HQMP molecule on the carbon steel surface. The quantum chemical parameters such as E_{HOMO}, E_{LUMO}, the energy gap ΔE (E_{LUMO} - E_{HOMO}), and dipole moment (μ) were obtained for the neutral HQMP molecule to predict their activity toward metal surface. These quantum chemical parameters were generated after geometric optimization with respect to all nuclear coordinates. Figure 15 shows the optimized geometry of HQMP. Frontier orbital density distribution is useful in predicting adsorption centers of the HQMP molecule responsible for the interaction with metal surface atoms. Figure 16 shows the HOMO and the LUMO density

distribution of HQMP. It is seen that the distribution of two energies HOMO and LUMO, we can see that the electron density of the HOMO and LUMO location was distributed almost of the entire molecule. The calculated molecular parameters are listed in Table 4.

According to frontier orbital theory, the reaction of reactants mainly occurred on the highest occupied molecular orbital (HOMO) and lowest unoccupied molecular orbital (LUMO). The energy of HOMO (E_{HOMO}) is related to ionization potential while the energy of LUMO (E_{LUMO}) is directly related to electron affinity. Higher values of E_{HOMO} indicate a tendency of the inhibitor molecules to donate electrons to appropriate acceptor molecules with low energy or empty 3d orbital of Fe to form coordinate bond [35]. The lower values of E_{LUMO}, the stronger the electron accepting ability of the inhibitor molecule, so that back-donating bond can be formed with its anti-bonding orbitals. From Table 4, the low value of dipole moment probably increases the adsorption between chemical compound and metal surface [36]. The adsorption of HQMP molecules from the aqueous solution can be regarded as a quasi-substitution process between the HQMP in the aqueous phase [$HQMP_{(sol)}$] and water molecules at the electrode surface [$H_2O_{(ads)}$]. Moreover, a smaller energy gap, ΔE (E_{LUMO}-E_{HOMO}) of 3,0205 (eV), a higher molecular weight, higher area and volume enhance effective adsorption of HQMP on the steel XC38 surface thus decreasing the corrosion rate of this metal.
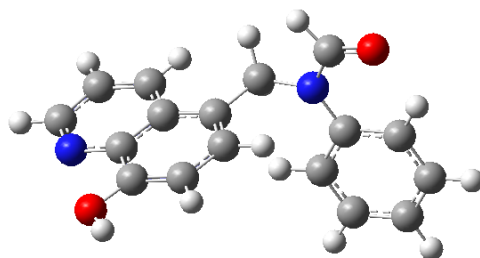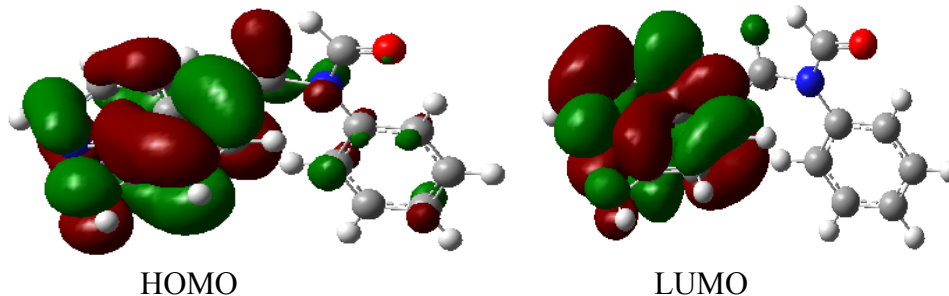

Figure 15: Optimized structures of HQMP

HOMO   LUMO

Figure 16: Frontier molecular orbital density distributions of HQMP

Table 4: Calculated Quantum Chemical Parameters of the HQMP

E_{HOMO} (eV)	E_{LUMO} (eV)	ΔE_{gap} (eV)	μ (debye)	IE (eV)	AE (eV)	ΔN
-8,6532	-5,6327	3,0205	1.544	8,6532	5,6327	0,04731

Conclusions

On the basis of the results obtained, it can be concluded that:
- The experimental results obtained from weight loss measurements, Polarization and impedance measurements studies are in good agreement.
- The inhibition efficiency of HQMP attains a maximum value of about 93 % at 10^{-4} M, the Polarisation measurements show that HQMP acts essentially as an anodic type inhibitor and this inhibition effect increases with the increase of concentration.
- The effectiveness of inhibition HQMP slowly decreases with temperature.
- Adsorption of HQMP tested follows Langmuir adsorption isotherm.
- Quantum calculations agree the efficiency values obtained.

References

1. Abdallah M., Helal E. A., Fouda A. S*., Corros. Sci.* 48 (7) (2006) 1639-1654.
2. El-Maksoud S. A., *Int. J. Electrochem. Sci.* 3 (2008) 528 - 555.
3. Alsabagh A. M., Migahed M. A., Awad H. S.,*Corros. Sci.* 48 (2006) 813-828.
4. Belayachi M., Serrar H., El Assyry A., Oudda H., Boukhris S., Touhami M. E., Zarrouk A., Hammouti B., Ebenso Eno E., El Midaoui A., *Int. J. Electrochem. Sci.* 10 (2015) 3038-3053
5. Boudalia M., Sebbar N.K., Bourazmi H., Lahmidi S., Ouzidan Y., Essassi E.M., Tayebi H., Bellaouchou A.,   Guenbour A., Zarrouk A., *J. Mater. Environ. Sci.* 7 (3) (2016) 878-888.
6. El Assyry A., Benali B., Lakhrissi B., El Faydy M., Touhami M. E., Touir R., Touil M., *Res. Chem. Intermed.* 41 (2013) 3419-3431
7. Tourabi M., Nohair K., Nyassi A., Hammouti B., Chetouani A., Bentiss F., *Mor. J. Chem.*, 1 (2013) 33-46.
8. Zarrouk A., Zarrok H., Salghi R., Hammouti B., Bentiss F., Touir R., Bouachrine M., *J. Mater. Environ. Sci.* 4 (2013)177-192.
9. Sebbar N. K., Elmsellem H., Boudalia M., Lahmidi S., Belleaouchou A., Guenbour A., Essassi E.M., Steli H., Aouniti A., *J. Mater. Environ. Sci.* 6 (11) (2015) 3034-3044.
10. Ganesha Achary H.P. Sachin Y. Arthoba Naik T.V. Venkatesha, *Mater. Chem. Phys.* 107 (2008) 44–50.
11. Tayebi H., Bourazmi H., Himmi B., El Assyry A., Ramli Y., Zarrouk A., Geunbour A., Hammouti B., Ebenso E. E., *Der Pharmacia Lettre* 6 (6) (2014) 20-34
12. El Faydy M., Dahaief N., Rbaa M., Ounine K., Lakhrissi B., *J. Mater. Environ. Sci.* 7 (1) (2016) 356-361
13. Haynes W. M., *CRC Handbook of chemistry and physics, Boca Raton, CRC Press/Taylor and Francis*, 91e éd (2011) 2610.
14. Ma H., Chen S., Liu Z., Sun Y, *J. Mol. Struct. (Theochem)* 774 (2006) 19-22.
15. Henríquez-Román J. H., Padilla-Campos L., Páez M. A., Zagal J. H., Rubio M. A., Rangel C. M., Costamagna J., Cárdenas-Jirón G., *J. Mol. Struct. (Theochem)* 757 (2005) 1-7.
16. Rodriguez-Valdez L. M., Martínez-Villafañe A., Glossman-Mitnik, D., *J. Mol. Struct. (Theochem)* 713 (2005) 65-70.
17. Feng Y., Chen S., Guo W., Zhang Y., Liu G., *J. Electroanal. Chem.* 602 (2007) 115-122.
18. Frisch M., Trucks G. W., Schlegel H. B., Scuseria G. E., Robb M. A., Cheeseman J. R.,. et al., Gaussian 03, Revision E.01, Gaussian, Inc., Wallingford CT (2004).
19. Dewar M. J., Thiel W., *J. Am. Chem. Soc.* 99 (1977) 4899-4907.
20. Pearson R. G., *Inorg. Chem.* 27 (1988) 734-740.
21. Yadav M., Behera D., Kumar S., Sinha R. R., *Ind. En. Chem. Res.* 52(19) (2013) 6318-6328.
22. Lukovits I. , Kalman E., Zucchi F., *Corrosion (NACE)* 57 (2001) 614–620.
23. Kumari P. P., Rao S. A., Shetty P., *Procedia Mater. Sci.* 5 (2014) 499-507.
24. El-Hajjaji F., Zerga B., Sfaira M., Taleb M., Ebn Touhami M., Hammouti B., Al-Deyab S.S., Benzeid H., Essassi El M., *J. Mater. Environ. Sci.* 5 (2014) 255-262.
25. Benali O., Larabi L., Traisnel M., Gengembra L., Harek Y., *Appl. Surf. Sci.* 253 (2007) 6130-6137.
26. Quraishi M. A., Rawat J., *Mater. Chem. Phys.* 70 (2001) 95-102.
27. Hammouti B., Zarrouk A., Al-Deyab S. S., Warad I., *Orient. J. Chem.* 27(2011), 23-31.
28. Abiola O. K., *Corros. Sci* 48 (10) (2006) 3078-3090.
29. Oguzie E. E., *Corros. Sci.* 49 (3) (2007) 1527- 1539.
30. Banera M. J., Caram J. A., Gervasi C. A., Mirífico M. V*., J. Appl .Electrochem*, 44 (2014) 1337-1344.
31. Kustu C., Emregul K. C., Atakol O., *Corros. Sci.* 49 (2007) 2800- 2814.
32. Li W., He Q., Pei C., Hou B., *Electrochim. Acta* 52 (2007) 6386-6394.
33. Selvakumar P., Balanaga Karthik B., Thangavelu C. *J. Mater. Environ. Sci.* 5 (6) (2014) 1750-1757.
34. Guadalupe H.J., Garcia-Ochoa E., Maldonado-Rivas P.J., Cruz T., Pandiyan J., *J. Electroanal. Chem.* 655 (2011) 164-172.
35. Obot I. B., Obi-Egbedi N. O., *Mater. Chem. Phys.* 122 (2010) 325-328.
36. Vijayakumar S., Kolandaivel P*., J. Mol. Struct.* (*Theochem*) 770 (2006) 23-30.

(2016); http://www.jmaterenvironsci.com/